The Journal of Chemical Physics

RESEARCH ARTICLE | JUNE 02 2022

Effective single component description of steady state structures of passive particles in an active bath

Jay Prakash Singh ✉; Sudipta Pattanayak; Shradha Mishra; ... et. al

J. Chem. Phys. 156, 214112 (2022)
https://doi.org/10.1063/5.0088259

The Journal of Chemical Physics ARTICLE scitation.org/journal/jcp

Effective single component description of steady state structures of passive particles in an active bath

Cite as: J. Chem. Phys. 156, 214112 (2022); doi: 10.1063/5.0088259
Submitted: 15 February 2022 • Accepted: 15 May 2022 •
Published Online: 2 June 2022

Jay Prakash Singh,[1,a] Sudipta Pattanayak,[2,b] Shradha Mishra,[1,c] and Jaydeb Chakrabarti[3,d]

AFFILIATIONS

[1] Department of Physics, Indian Institute of Technology (BHU), Varanasi 221005, India
[2] Laboratoire de Physique Théorique et Modélisation, CNRS UMR 8089, CY Cergy Paris Université, 95302 Cergy-Pontoise, France
[3] S. N. Bose National Centre for Basic Sciences, JD Block, Sector III, Salt Lake City, Kolkata 700106, India

[a] **Author to whom correspondence should be addressed:** jayps.rs.phy16@itbhu.ac.in
[b] pattanayak.sudipta@gmail.com
[c] smishra.phy@iitbhu.ac.in
[d] jaydeb@bose.res.in

ABSTRACT

We model a binary mixture of passive and active Brownian particles in two dimensions using the effective interaction between passive particles in the active bath. The activity of active particles and the size ratio of two types of particles are the two control parameters in the system. The effective interaction is calculated from the average force on two particles generated by the active particles. The effective interaction can be attractive or repulsive, depending on the system parameters. The passive particles form four distinct structural orders for different system parameters, viz., homogeneous structures, disordered cluster, ordered cluster, and crystalline structure. The change in structure is dictated by the change in nature of the effective interaction. We further confirm the four structures using a full microscopic simulation of active and passive mixture. Our study is useful to understand the different collective behavior in non-equilibrium systems.

I. INTRODUCTION

A complex system, in general, has a host of degrees of freedom out of which only a finite subset could be of interest to describe certain properties of the system. Such a reduced description, also known as the effective free energy description in terms of a set of selected degrees of freedom while integrating the remaining degrees of freedom of the system, is a well-established technique in equilibrium.[1] Depletion forces between hard sphere colloids in dispersion belong to this category, for instance.[2] Since many of the equilibrium techniques, including a free energy based description, break down for a system out of equilibrium,[3] a reduced description of such systems in analogy to equilibrium is not obvious. In attempting reduced description of a system out of equilibrium,[4,5] hydrodynamic continuum equations for phase separation in active Brownian particles are developed based on the symmetries and conservation laws of the system. To the best of our knowledge, studies based on the effective force have not been attempted for non-equilibrium systems. Such a description based on effective forces does not have either of the extremities, neither as much coarse-grained as in the continuum approach nor having all the detailed microscopic degrees of freedom in the system.

Non-equilibrium systems exhibit a variety of collective behaviors. A collection of active or self-propelled particles[6–10] is of current interest, where the system is driven out of equilibrium. Examples of active systems range from small scale of the order of intracellular to macroscopic length scale of few meters,[6,11–26] exhibiting a host of non-equilibrium phenomena, such as pattern formation,[13] non-equilibrium phase transition,[27] large density fluctuations,[28–31] enhanced dynamics,[32–40] motility[41–45] induced phase separation,[47–51] transport phenomenon,[52,53] and so on. Collection of spherically symmetric active Brownian particles (ABP), such as the Janus particles, or active colloids shows motility induced

phase separation (MIPS) at a packing density much lower than their equilibrium counterparts.[54] Recently, MIPS has been extensively studied in various experiments on synthetic colloids, and bacterial and cell suspensions.[47–49,51] Recent advancement on MIPS for pure ABPs without alignment shows the emergence of spatial velocity correlations, affecting spatial organization of the ABPs.[55,56] Motivated by the MIPS in pure active systems, the mixture of passive and active particles has also been explored in various experiments and theoretical studies.[13,32] There are reports on the phase separation of passive particles by varying system parameters, such as the activity of the medium and size of passive particles.[57–60] Phase separation of passive particles in the mixture can be a potential model to explore the clustering and aggregation of macro-molecules in a cellular environment.[61–67]

As a prototype of collective behavior in systems out of equilibrium, it is interesting to develop a reduced description of the MIPS. In equilibrium, the effective interaction among the solute particles in a bath of solvent particles is measured in terms of the pair correlation function of solvent particles $g_2(r)$[58,68–69] or from the average force acting by the solvent particles on two solute particles at a fixed separation.[70–76] There are recent reports on non-equilibrium depletion forces.[77–85] It has been shown in Ref. 77 that the effective force between passive particles in an active medium cannot be accounted for in terms of $g_2(r)$. In addition, the solvent mediated average force on two solute particles depends on the manner in which particles are constrained. Both the features suggest departure from the equilibrium scenario. Unlike the equilibrium counterpart, it is not established, yet to the best of our knowledge, how far the effective interaction in these out of equilibrium systems can describe the collective behavior in steady state.[58]

In this study, we focus on the steady state spatial organization of the passive particles in the presence of ABPs in terms of the effective potential between two passive particles in the bath. We fix the passive particles at a given separation, while the ABPs perform their motions. The component of the forces between the active and passive particles along the separation vector of the fixed passive particles is computed and averaged over many steady state configurations to give the effective interaction between the passive particles. We perform Brownian dynamics simulations with a large number of passive particles with the effective potential to determine different steady state structures of the passive system. We are thus left with an effective single component system of the passive particles alone without the ABPs where the active degrees of freedoms are integrated out into the effective interaction. We observe four different structural orders of the passive particles in parameter space, spanned by the size ratio and activity of passive and active particles: (i) homogeneous structure (HS), (ii) disorder-cluster (DC), (iii) ordered cluster (OC), and (iv) crystalline structure (CS). Finally, observed structures of passive particles are confirmed by the full microscopic simulation of a binary mixture of active and passive particles.

In the rest of the paper, we discuss the details of the binary model system in Sec. II. Section III A discusses the result of effective force between two passive particles in the presence of small ABPs. In Sec. III B, we show the effect of the effective force on a purely passive system and the characteristics of four structures are discussed in detail. Finally, we conclude the paper with a summary and discussion in Sec. IV.

II. MODEL

Our system consists of a binary mixture of N_a ABPs of radius r_a and N_p passive particles of radius r_p moving in two dimensions $L_x \times L_y$ with the periodic boundary conditions. We define size ratio of the particles $S = r_p/r_a$. Let us represent the position vector of the center of the ith ABP and passive particles by $\mathbf{r}_i^a(t)$ and $\mathbf{r}_i^p(t)$, respectively, at time t. The orientation of ith ABP is represented by a unit vector $\mathbf{n}_i(t) = (\cos\theta_i(t),\ \sin\theta_i(t))$. The dynamics of the active particle is governed by the overdamped Langevin equation

$$\partial_t \mathbf{r}_i^a = v\mathbf{n}_i + \mu_1 \sum_{j\neq i} \mathbf{F}_{ij}, \tag{1}$$

$$\partial_t \theta_i(t) = \eta_i^r(t). \tag{2}$$

The first term on the right-hand side (RHS) of Eq. (1) is due to the activity of the ABPs with active self-propulsion speed v. The rate of change of the orientation θ_i of the ith ABP is given by Eq. (2). The stochastic force $\eta_i^r(t)$ at time t is defined as $\langle \eta_i^r(t)\eta_j^r(t')\rangle = 2\nu_r\delta_{ij}\delta(t-t')$. ν_r represents the rotational diffusion constant. The persistence length of the ABPs is defined as $l = v/\nu_r$, and the corresponding persistent time $\tau = 1/\nu_r$. We define the dimensionless activity as $\tilde{V} = \frac{v}{r_a\nu_r}$. The rotational diffusion constant is kept fixed at $\nu_r = 0.005$. The size of the active particles $r_a = 0.1$. The force term $\mathbf{F}_{ij}$ in both equations is due to soft repulsive steric interaction between the particles, $\mathbf{F}_{ij} = -\nabla U(r_{ij})$, where $U(r_{ij}) = k(r_{ij} - (r_{\beta i} + r_{\beta' j}))^2$ if $r_{ij} \leq (r_{\beta i} + r_{\beta' j})$ and r_β is the radius of active or passive particles for β and $\beta' = a$ or p, respectively. The mobility of active particles are kept as $\mu_1 = 1.0$ and the force constant $k = 1.0$; hence, $(\mu_1 k)^{-1} = 1.0$ defines the elastic time scale in the system. The area fraction of the ABPs is $\phi_a = N_a\pi r_a^2/(L_x \times L_y)$ and kept fixed at $\phi_a = 0.5$. The area fraction of passive particles depends on the size of passive particles. The smallest time step considered is $\Delta t = 0.001$. The size ratio S and dimensionless activity $\tilde{V}$ are the two control parameters and they are varied from (1 to 10) and (20 to 160), respectively.

In order to calculate the effective potential between two passive particles, we choose $N_p = 2$ at positions $\vec{R}_1$ and $\vec{R}_2$, respectively, in the sea of ABPs ($N_a = 1000$). We keep $\vec{R}_1$ fixed and slowly vary $\vec{R}_2$ in small steps of $\delta x = 1.5r_a$ starting from the zero surface to the surface distance between two passive particles. The active particle coordinates are updated according to Eqs. (1) and (2). For each configuration at a given distance between two passive particles, the system is allowed to reach the steady state. Typical time for the steady state $\tau = 5 \times 10^7$. Furthermore, we use the steady state configuration to calculate the force $\mathcal{F}^{S,\tilde{V}}(r)$ between two passive particles at a surface to surface separation r, such that $\mathcal{F}^{S,\tilde{V}}(r) = \mathbf{F}_{12}(r) + \sum_{i=1}^{N_a}\mathbf{F}_{1i}(r)$. Here, $\mathbf{F}_{12}(r)$ is the force due to the passive particle second on the first, and $\sum_{i=1}^{N_a}\mathbf{F}_{1i}(r)$ represents the sum of all the forces due to active particles on the first passive particle for a given configuration of two passive particles at separation r. Then, the potential is calculated by integrating the force over the distance $V^{eff}(r) = \int_{-\infty}^{r}\mathcal{F}^{S,\tilde{V}}(r)dr$.[70,71] Here, we set the lower limit as half of the box-length. To improve the quality of data, 200 independent realizations of the similar system is designed. We have measured the system potential energy with respect to the time to ensure approach to steady state.

Now, we define the coarse-grained model to study the system with effective potential $V^{eff}(r)$. Here, the system consists of a collection of passive particles only without any ABPs, interacting with the force $\mathcal{F}^{S,\tilde{V}}(r)$ calculated from the effective potential. We take $N_p = 400$ in two dimensions with linear dimensions $L_x = L_y = 800r_a$ with the periodic boundary conditions in both the directions. Here, the size of the passive particles is kept the same as for the corresponding potential $V^{eff}(r)$ obtained from the binary system. Hence, the area fraction of particles ϕ_p is different for the different ranges of potential used. The position update of passive particles in the coarse-grained simulations is given by the over-damped Langevin equation

$$\partial_t \mathbf{r}_i^p = -\mu_2 \sum_{j\neq i} \nabla V_{ij}^{eff}(r) + \sqrt{2D_T}\eta_i^R(t). \tag{3}$$

The first term on the right-hand side (RHS) of Eq. (3) defines the effective interaction force between the passive particles pair i and j, where r is the surface to surface separation between ith and jth passive particles. The translational noise $\eta_i^R(t)$ at time t is defined as $\langle \eta_i^R(t)\eta_j^R(t')\rangle = \delta_{ij}\delta(t-t')$. $D_T = 1.0$ represents the translational diffusion constant. The mobility of passive particles is taken as $\mu_2 = 2\times10^{-2}$. All other parameters are the same as defined in Sec. II. We consider the total simulation time steps $t = 5\times10^6$. All the physical quantities calculated here are averaged over 50 realizations of the random noise. Other details are the same as discussed previously. The system is simulated for potentials obtained for the different combination of S and $\tilde{V}$. Here, the steady state is also judged based on the potential energy fluctuations.

III. RESULTS AND DISCUSSIONS

A. Effective potential between passive particles

A schematic of the system at a fixed surface–surface separation (r) of passive particles is shown in Fig. 1. The results for the

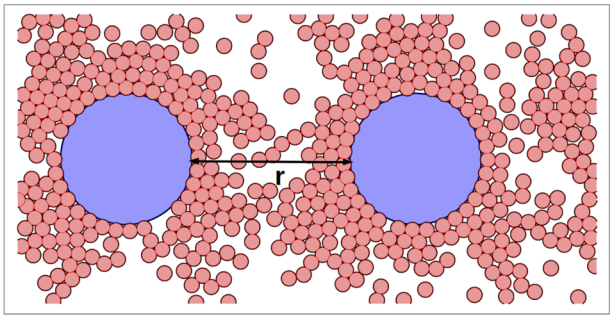

FIG. 1. Plot showing the model picture of small ABPs and big passive particles with size ratio $S = 10$ to calculate the effective potential $V^{eff}(r)$ on passive particle separated by distance "r" exerted by the active depletant. Blue and red particles show passive particles and ABPs. The black arrowed line shows the surface to surface distance "r" between two passive particles. The number of ABPs and passive particles are $N_a = 1000$ and $N_p = 2$, respectively.

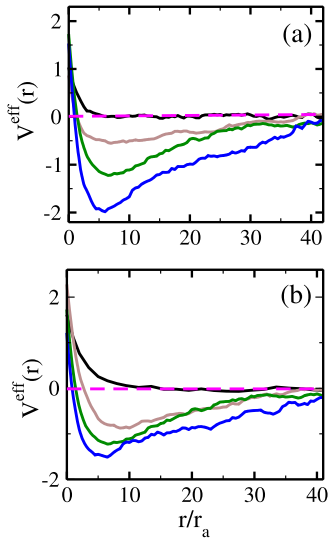

FIG. 2. In this panel, we show the variation of numerically obtained active depletant potentials $V^{eff}(r)$ on passive particles for various $\tilde{V}$ and size ratio S, where $\frac{r}{r_a}$ is the passive particles separation distance from surface to surface normalize by the ABP radius r_a. Panel (a) shows the variation of potentials with colors black, brown, green, and blue lines keeping fixed $\tilde{V} = 160$ for $S = 4$, 5, 8, and 9, respectively. Panel (b): black, brown, green, and blue lines represent the variation of potentials for different $\tilde{V} = 40, 80, 120$, and 160, for fixed $S = 10$. The magenta line shows the reference line for the mean potential zero. The number of ABPs and passive particles are $N_a = 1000$ and $N_p = 2$, respectively.

effective potential $V^{eff}(r)$ vs scaled surface–surface distance between two passive particles $\frac{r}{r_a}$ are shown in Figs. 2(a) and 2(b) for different combinations of activity $\tilde{V}$ and size ratio S, respectively. Let us first discuss the results in Fig. 2(a). For a fixed $\tilde{V} = 160$ and small $S(=4)$, the potential is purely repulsive for small $\frac{r}{r_a}$ and then smoothly decay to zero for large $\frac{r}{r_a} \sim 40$. As we increase $S(>4)$, the potential becomes attractive with minimum at an intermediate distance and approaches zero value for large distances. Furthermore, the range and the depth of the attractive minima increases with increasing S. Similarly, we show $V^{eff}(r)$ for different $\tilde{V}$ at a fixed $S = 10$ in Fig. 2(b). For small $\tilde{V} = 40$, the potential is purely repulsive for small distances $\frac{r}{r_a}$ and then approaches zero at large distances. As we increase $\tilde{V}$, the potential starts to develop attractive minima at moderate distances and then approaches zero at larger $\frac{r}{r_a}$. The depth of attractive minima and range of interaction increases on increasing $\tilde{V}$.

B. Steady state structural crossover

We extract the steady state structure of the pure passive particles with $V^{eff}(r)$. Note that the active bath particles are not explicitly considered in these simulations. We show a representative particle snapshot on the left-hand panels for structurally distinct configurations. The radial correlation functions, $g_2(r)$, given by the distribution of the pair separations between the particles in the system, are shown on the right-hand side panel corresponding to the snapshot. We find the following four structures of passive particles:

1. Homogeneous structure (HS)

Here, isolated passive particles are homogeneously distributed for $(S, \bar{V}) = (4, 160)$ as shown in Fig. 3(a). Figure 3(b) shows the radial correlation function $g_2(r)$ vs $\frac{r}{r_p}$. The $g_2(r)$ shows a single peak at the diameter of the particle and then decay monotonically at larger distances, confirming the homogeneous structure.

2. Disordered clusters (DC)

The passive particles form big clusters, but the particles are distributed randomly within the cluster, as shown in the representative snapshot in Fig. 3(c) for $(S, \bar{V}) = (5, 160)$. The right plot in Fig. 3(d) that $g_2(r)$ bears signature of short ranged positional order.

3. Ordered cluster (OC)

The particles are arranged in big clusters with local hexagonal order for $(S, \bar{V}) = (10, 160)$, as shown in Fig. 3(e). The $g_2(r)$ data show the strong periodic peaks. The location of second and third peaks appears at $\sqrt{3}$ and two times the location of the first peak as shown in Fig. 3(f), consistent with the hexagonal packing. The hexagonal packing is absent in the clusters of DC structure.

4. Crystalline structure (CS)

The passive particles form long range ordered domains with primarily six-coordinated particles. There are small amount of defects (2%–3%) having particles of 5-fold or 7-fold coordination, as shown in the snapshot of Fig. 3(g) for $(S, \bar{V}) = (10, 40)$. The $g_2(r)$ plot in Fig. 3(h) shows spilt first peak and rather broad higher peaks, suggesting a long ranged order with defects. A detailed discussion has been given in the supplementary material, Fig. 1.

Next, we quantify the cluster size distribution in the system for different structures in the steady state. A cluster is defined as a set of particles connected by a most probable distance r_0. We define the fraction of cluster of size n as the cluster size distribution (CSD) $P(n)$. The normalized $P(n)$ for different states are shown in Figs. 4(a)–4(d) in the log–log scale. In the D structure, $P(n)$ in Fig. 4(a) shows small clusters. For the DC structure in Fig. 4(b), $P(n)$ shows an additional peak around for finite size, following which there is a steep decay $n^{-3.5}$ for large n. The peak for larger n gets prominent for OC and CS, shown in Figs. 4(c) and 4(d), respectively.

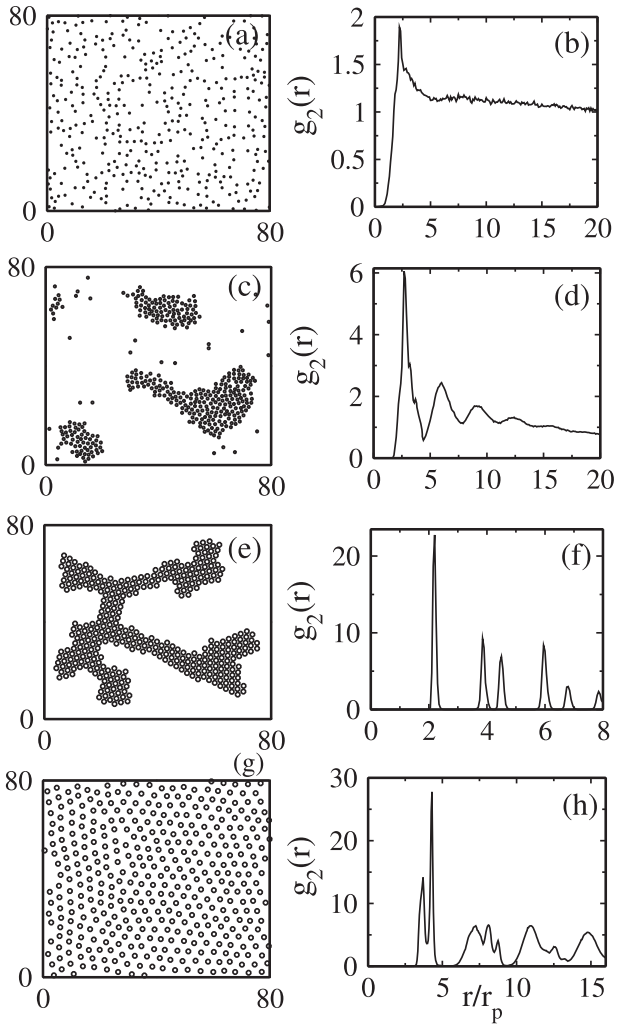

FIG. 3. Plots (a), (c), (e), and (g) show the steady state snapshots for the four structures of the passive particles interacting through the potential obtained with different combinations of activity $\bar{V}$ and size ratio S shown in Fig. 2. (a) Homogeneous structure (HS) for $S, \bar{V} = 4, 160$, (c) disorder cluster (DC), for $S, \bar{V} = 5, 160$, (e) ordered cluster (OC) for $S, \bar{V} = 10, 160$, and (g) crystalline structure (CS) for $S, \bar{V} = 10, 40$. In the right panel top to bottom (b), (d), (f), and (h), we show the radial correlation function $g_2(r)$ vs r/r_p for the same values of $\bar{V}$ and S in the given structures discussed in panels (a), (c), (e), and (g), respectively. The number of passive particles $N_p = 400$.

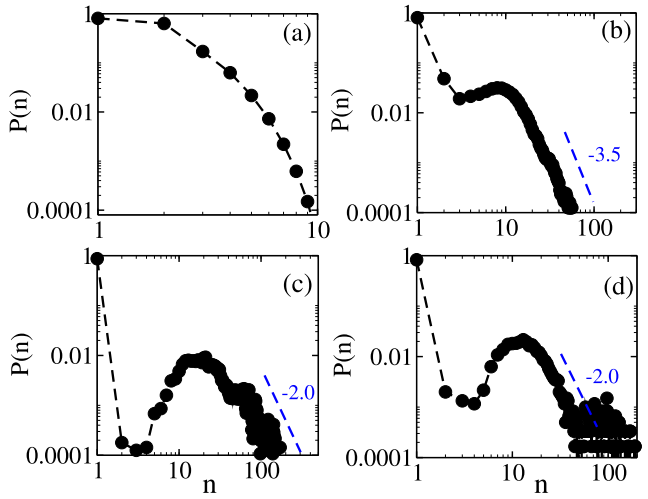

FIG. 4. We plot cluster size distribution CSD $P(n)$ vs mean number of particles n for four distinct structures. In panel (a), for homogeneous structure (HS), we show the CSD for fixed $S = 4$ and activity $\bar{V} = 160$. (b) Disorder cluster (DC): for fixed $\bar{V} = 160$ and size ratio $S = 5$. (d) Ordered Cluster (OC): $\bar{V} = 160$ and $S = 10$. (c) Crystalline structure (CS): for fixed $\bar{V} = 40$ and size ratio $S = 10$. In the homogeneous structure, CSD decays exponentially, while in the crystalline and order cluster, CSD decay with power law with exponent −2.0. Furthermore, for the disorder cluster, CSD decays with the power of exponent −3.5. The number of passive particles $N_p = 400$.

The tail of $P(n)$ decays less steeply than the DC state, with the power law exponent −2.0.

We characterize the steady state structures employing (1) the size of the largest cluster m and (2) the bond orientation order parameter ψ_6.[86,87] The bond orientation order parameter is expressed in terms of angular correlations between a vector defined in terms of spherical harmonics that identify the local environment around a central particle.[86,87] In 2D, the bond orientation order parameter ψ_6 is defined as

$$\psi_6 = \frac{1}{N_p}\sum_{k=1}^{N_p}\sqrt{\frac{1}{N_k}\sum_{j=1}^{N_k} e^{i6\theta_{kj}}}, \tag{4}$$

where N_p is the total number of passive particles and N_k shows the number of particles in the neighbor of jth particle. θ_{kj} is the angle between the bond connecting the kth and jth particles. $\psi_6 \sim 0$ and $\psi_6 \sim 1.0$ describe the disordered and perfect hexagonal packed structure, respectively. The values of m and ψ_6 are shown in Table I for cases in Fig. 3. The error bars in the number shows the range of m and ψ_6 for different S and $\bar{V}$, where the similar structures are found. The m and ψ_6 values suggest that CS have cluster size and orientation order in between OC and DC and are not structurally distinct.

In Fig. 5(a), we show the variation of m with S for different $\bar{V}$. We find that m shows a jump to large values beyond a S_c, a critical value of S. The inset shows that S_c decreases linearly with $\bar{V}$. This suggests that larger $\bar{V}$ favors the formation of larger clusters. We show in Fig. 5(b) the variation of ψ_6 as a function of S for different $\bar{V}$. We observe that a long-ranged crystalline order is set up above S_c for different $\bar{V}$ with a small jump in the order parameter value. The inset shows that S_c based on ψ_6 does not show strong sensitivity on $\bar{V}$, unlike that determined from the magnitude of m. This suggests that the formation of a large cluster is sensitive to $\bar{V}$, but the orientation order is primarily sensitive to S.

Next, we consider the full steady state structural crossover diagram to approximately demarcate the boundaries in $S-\bar{V}$ plane, as shown in Fig. 5(c), based on the values of m and ψ_6. The crossover diagram is divided broadly into two regions by the solid line where region HS represents the homogeneous region, while the region above the solid line shows different clustered regions (OC and DC) divided by dashed lines. The HS region is characterized by small m along with small ψ_6. The DC structure corresponds to large $m(60)$ but small ψ_6, while the OC structures correspond to large values of both. The disordered structure crosses over to clusters for sufficiently large S for a given $\bar{V}$. The boundary shifts to lower S with increasing $\bar{V}$, which is consistent with the data in the inset of Fig. 5(a). The disordered clusters get ordered one where the boundary is independent of (S) as observed in the inset of Fig. 5(b). On the other hand, for large S and low $\bar{V}$, the disordered structure crosses over to crystalline (CS) domains.

TABLE I. Characterization of structures with respect to m and ψ_6.

Structures	m	ψ_6
HS	8.0 ± 5	0.05 ± 0.012
DC	75.0 ± 20	0.3 ± 0.120
OC	170.0 ± 25	0.70 ± 0.100
CS	138.0 ± 20	0.63 ± 0.15

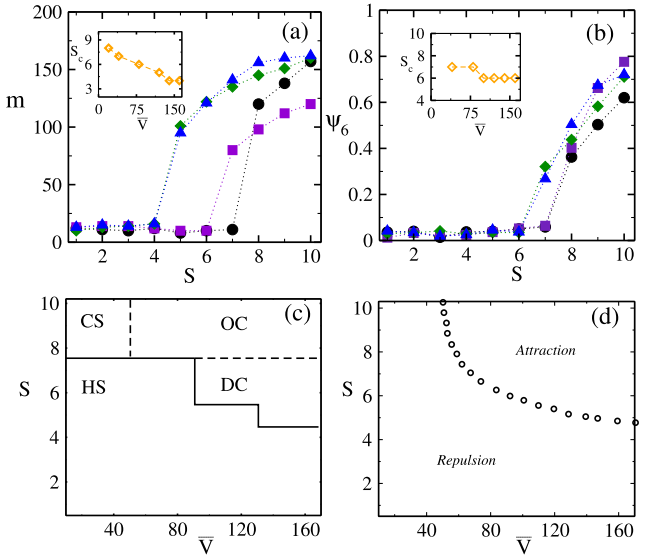

FIG. 5. In panel (a), we show the mean cluster size m vs S, where black circles, violet squares, green diamonds, and blue triangles represent different $\bar{V} = 40, 80, 120$, and 160, respectively. Inset: (a) shows the variation of critical size S_c vs $\bar{V}$ with respect to mean size m. Panel (b) represent variation of ψ_6 vs S, where black circles, brown squares, green diamonds, and blue triangles represent different $\bar{V} = 40, 80, 120$, and 160, respectively. Inset (b) shows the variation of critical size S_c vs $\bar{V}$ with respect to the mean bond orientation order parameter ψ_6. (c) We show the full phase diagram of four different structures in S–$\bar{V}$ plane, taking care the restrictions over ψ_6 and m. Dashed lines show the phase coexistent between two states. (d) shows the nature of effective interaction in $S-\bar{V}$ plane. In all the plots, the number of passive particles is 400.

It may be important to point out that the structural crossover suggests mutual adjustment of particle positions in response to the change in the effective interaction. Thus, it is interesting to correlate the crossover boundaries to the changes in the nature of $V^{eff}(r)$. The boundary between repulsive and attractive $V^{eff}(r)$ is shown in Fig. 5(d). $V^{eff}(r)$ is repulsive for low $\bar{V}$. However, for larger $\bar{V}$ where the ABPs undergo a large number of collisions while the passive particles change mutual separation, there is a crossover from repulsive interaction for low S to attractive interaction for larger S. The depletion mediated[33,34] force is an effective attraction between particles for large size differences with the bath particles in equilibrium. This is in sharp contrast to the change in the nature of the effective potential we observe in $S-\bar{V}$ plane in non-equilibrium conditions. The homogeneous structure is favored in the steady state for effective repulsion between the passive particles, while the clusters are favored when the interaction is attractive.

The crossover from the homogeneous structure to the crystalline domains takes place even if the interaction remains repulsive

in the low $\bar{V}$ regime. In this regime, τ is large so that the separation variable of the passive particles as a dynamical variable is more strongly coupled to the dynamics of the ABPs. Both the strength and the range of repulsive interaction increase with S and hence larger effective Barker–Henderson hardcore diameter.[88] This leads to better packing among the passive particles that leads to partial orientation order in the system. The orientation order in this regime is purely a steady state effect as the system parameters are far from order formation in equilibrium. We also check that the variances of the potential energy ΔU, governing the specific heat in equilibrium, do not show any characteristic peak, ruling out thermodynamic phase transition, as shown in the supplementary material, Fig. 2.

We further ensure that the two-body forces are dominant compared to the effective triplet interaction among the passive particles. Since we get predominantly triangular particle configurations in the simulations, we consider, for simplicity, symmetric triplet configurations as in Ref. 89. The details of calculations are given in the supplementary material. We find that the effective triplet force is less compared to the effective two-body forces at least for small separation, as shown in the supplementary material, Fig. 4. For large separation, however, the two contributions are similar. Since the structural organizations are primarily governed by the interaction at smaller distance, the structural crossovers are expected to be robust.

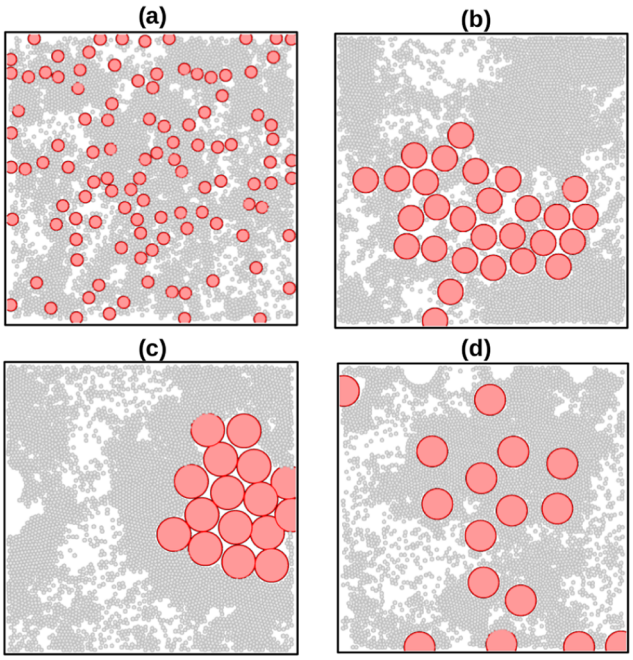

FIG. 6. Plots (a)–(d) show the four distinct structures obtained from microscopic simulation of ABPs and passive mixture with packing fraction $\phi_a = 0.5$ and $\phi_p = 0.2$. The parameters $\bar{V}$ and S are chosen from the phase diagram for four structures shown in Fig. 5(c). (a) represents the homogeneous structure (HS) for $(S, \bar{V}) = (4, 160)$. (b) shows the disorder cluster (DC) for $(S, \bar{V}) = (7, 160)$. (c) shows the order cluster (OC) for $(S, \bar{V}) = (10, 160)$. (d) represents crystalline structure (CS) for $(S, \bar{V}) = (9, 40)$. Smaller gray particles are ABPs, and red are passive ones.

C. Full microscopic simulations

Furthermore, the robustness of the structural organizations from the simulations employing the two-body forces is checked against full microscopic simulations of a mixture of active and passive particles with $\phi_a = 0.5$ and $\phi_p = 0.2$. In these simulations, we introduce the full microscopic interaction between the active and passive particles. Furthermore, the dimension has been taken as $L_x = L_y = 800 r_a$ with periodic boundary conditions in both directions. The position and orientation updates of ABP are given by Eqs. (1) and (2), and passive particles are updated using the following equation:

$$\partial_t \mathbf{r}_i^p = \mu_2 \sum_{j \neq i} \mathbf{F}_{ij}. \tag{5}$$

Other simulation details are as discussed in the model section. The system is simulated for total time steps of $t = 10^7$. The steady state structures of passive and active particles are observed in the steady state for different size ratios S and activity $\bar{V}$. We show in Fig. 6 four structures obtained by the full microscopic simulation of passive particles in the sea of the active particles. Figures 6(a)–6(d) represent the HS, DC, OC, and CS for the parameters S, $\bar{V} = (4, 160), (7, 160), (10, 160)$, and $(9, 40)$, respectively. The snapshots closely resemble the four structures of a purely passive system in the coarse-grained simulation. Hence, results obtained from the coarse-grained simulations of purely passive particles mixture are consistent with the results obtained for the full microscopic simulation of a binary mixture of active and passive particles. Thus, the forces from higher order particle configurations are not as significant as the pair-wise forces.

IV. CONCLUSION

We have studied a reduced model for steady state structural crossover of large passive particles in a bath of small Brownian active particles in two dimensions using the Langevin dynamics simulations. The effect of the active particle bath is taken into account through the two body effective potential between the passive particles. The activity $\bar{V}$ and the size ratio S are the two main control parameters in the system. We observe four different steady state structures of passive particles, namely, HS, DC, OC, and CS, distinguished by the largest cluster size and the bond orientation order parameter. Finally, full microscopic simulations for the binary mixture of active and passive particles reproduce the four structures. This shows that the single component effective potential reproduces the structural features.

Our study can be useful to understand the collective behavior of passive particles in active baths, for example, crystallization of passive colloids, segregation of protein, bacterial suspensions, cell suspensions, paint industry, and so on. It will be interesting to study the dynamics of the effective single component system to arrive at a comprehensive understanding of a passive system in an active bath. We have considered only white noise in our studies. It may be interesting to include colored noise to get more interesting steady state behavior.

SUPPLEMENTARY MATERIAL

See the supplementary material for the following: defect analysis of long range ordered CS, variance of energy ΔU across different phases, and effective triplet force contribution.

ACKNOWLEDGMENTS

J. P. Singh and S. Mishra acknowledge the support and the resources provided by PARAM Shivay Facility under the National Supercomputing Mission, Government of India, at the Indian Institute of Technology, Varanasi. The computing facility at the Indian Institute of Technology (BHU), Varanasi, is gratefully acknowledged.

AUTHOR DECLARATIONS

Conflict of Interest

The authors have no conflicts to disclose.

DATA AVAILABILITY

The data that support the findings of this study are available within the article.

REFERENCES

[1] C. N. Likos, Phys. Rep. **348**(4–5), 267 (2001).
[2] Y. Mao *et al.*, Physica A **222**, 10–24 (1995).
[3] A. Y. Grosberg and J.-F. Joanny, Phys. Rev. E **92**, 032118 (2015).
[4] R. Wittkowski, A. Tiribocchi, J. Stenhammar, R. J. Allen, D. Marenduzzo, and M. E. Cates, Nat. Commun. **5**, 4351 (2014).
[5] S. Pattanayak, S. Mishra, and S. Puri, Phys. Rev. E **104**, 014606 (2021).
[6] T. Feder, Phys. Today **60**(10), 31 (2007).
[7] S. Pattanayak, J. P. Singh, M. Kumar, and S. Mishra, Phys. Rev. E **101**, 052602 (2020).
[8] J. P. Singh *et al.*, J. Phys. A: Math. Theor. **54**, 115001 (2021).
[9] E. M. Rauch, M. M. Millonas, and D. R. Chialvo, Phys. Lett. A **207**, 185 (1995).
[10] J. P. Singh *et al.*, J. Stat. Mech.: Theory Exp. **2021**, 083217.
[11] J. Toner, Y. Tu, and S. Ramaswamy, Ann. Phys. **318**, 170 (2005).
[12] S. Ramaswamy, Annu. Rev. Condens. Matter Phys. **1**, 323 (2010).
[13] M. C. Marchetti *et al.*, Rev. Mod. Phys. **85**, 1143 (2013).
[14] Y. Harada, A. Noguchi, A. Kishino, and T. Yanagida, Nature **326**, 805–808 (1987).
[15] M. Badoual, F. Jülicher, and J. Prost, Proc. Natl. Acad. Sci. U. S. A. **99**, 6696–6701 (2002).
[16] F. J. Nedelec, T. Surrey, A. C. Maggs, and S. Leibler, Nature **389**, 305–308 (1997).
[17] E. Ben-Jacob *et al.*, Phys. Rev. Lett. **75**, 2899–2902 (1995).
[18] M. C. Appleby, *Animal Groups in Tree Dimensions*, edited by J. K. Parrish, and W. M. Hamner (Cambridge University Press, Cambridge, 1997).
[19] D. Helbing, I. Farkas, and T. Vicsek, Nature **407**, 487–490 (2000).
[20] D. Helbing, I. J. Farkas, and T. Vicsek, Phys. Rev. Lett. **84**, 1240–1243 (2000).
[21] E. Kuusela, J. M. Lahtinen, and T. Ala-Nissila, Phys. Rev. Lett. **90**, 094502 (2003).
[22] S. Hubbard, P. Babak, S. T. Sigurdsson, and K. G. Magnússon, Ecol. Modell. **174**, 359–374 (2004).
[23] V. Schaller, C. Weber, C. Semmrich, E. Frey, and A. R. Bausch, Nature **467**, 73–77 (2010).
[24] Y. Sumino *et al.*, Nature **483**, 448–452 (2012).
[25] F. Peruani, Phys. Rev. Lett. **108**, 098102 (2012).
[26] E. Ben-Jacob, I. Cohen, O. Shochet, A. Tenenbaum, A. Czirók, and T. Vicsek, Phys. Rev. Lett. **75**, 2899 (1995).
[27] T. Vicsek *et al.*, Phys. Rev. Lett. **75**, 1226 (1995).
[28] G. Gregoire and H. Chate, Phys. Rev. Lett. **92**, 025702 (2004).
[29] H. Chate, F. Ginelli, G. Gregoire, and F. Raynaud, Phys. Rev. E **77**, 046113 (2008).
[30] B. Bhattacherjee, S. Mishra, and S. S. Manna, Phys. Rev. E **92**, 062134 (2015).
[31] V. Narayan, S. Ramaswamy, and N. Menon, Science **317**, 105 (2007).
[32] C. Bechinger, R. Di Leonardo, H. Lwen, C. Reich- hardt, G. Volpe, and G. Volpe, Rev. Mod. Phys. **88**, 045006 (2016).
[33] L. Angelani, R. Di Leonardo, and G. Ruocco, Phys. Rev. Lett. **102**, 048104 (2009).
[34] J. Harder, S. A. Mallory, C. Tung, C. Valeriani, and A. Cacciuto, J. Chem. Phys. **141**, 194901 (2014).
[35] S. Kumar, J. P. Singh, and S. Mishra, Phys. Rev. E **104**, 024601 (2021).
[36] P. de Castro and P. Sollich, Phys. Chem. Chem. Phys. **19**, 22509–22527 (2017).
[37] V. Semwal, J. Prakash, and S. Mishra, arXiv:2112.13015 (2021).
[38] S. Pattanayak, R. Das, M. Kumar, and S. Mishra, Eur. Phys. J. E **42**, 62 (2019).
[39] V. Semwal, S. Dikshit, and S. Mishra, Eur. Phys. J. E **44**, 20 (2021).
[40] A. Baskaran and M. C. Marchetti, Phys. Rev. Lett. **101**(26), 268101 (2013).
[41] S. Chaki and R. Chakrabarti, Physica A **530**, 121574 (2019).
[42] S. Chaki and R. Chakrabarti, Physica A **511**, 302–315 (2018).
[43] D. Frenkel and A. A. Louis, Phys. Rev. Lett. **68**, 3363 (1992).
[44] T. Biben and J.-P. Hansen, Phys. Rev. Lett. **66**, 2215 (1991).
[45] S. Asakura and F. Oosawa, J. Polym. Sci. **33**, 183 (1958).
[46] U. Kühn, Inf. Process. Lett. **68**, 307–312 (1998).
[47] I. Buttinoni, J. Bialké, F. Kümmel, H. Löwen, C. Bechinger, and T. Speck, Phys. Rev. Lett. **110**, 238301 (2013).
[48] M. E. Cates and J. Tailleur, Annu. Rev. Condens. Matter Phys. **6**, 219 (2015).
[49] E. Sesé-Sansa, I. Pagonabarraga, and D. Levis, Europhys. Lett. **124**, 30004 (2018).
[50] S. Dikshit and S. Mishra, arXiv:2108.08921 (2021).
[51] A. P. Solon, Y. Fily, A. Baskaran, M. E. Cates, Y. Kafri, M. Kardar, and J. Tailleur, Nat. Phys. **11**, 673 (2015).
[52] I. Santra and U. Basu, arXiv:2201.00796v1 (2022).
[53] O. Granek, Y. Kafri, and J. Tailleur, arXiv:2108.11970v2 (2022).
[54] Y. Fily and M. C. Marchetti, Phys. Rev. Lett. **108**, 235702 (2012).
[55] L. Caprini, U. Marini Bettolo Marconi, and A. Puglisi, Phys. Rev. Lett. **124**, 078001 (2020).
[56] L. Caprini, U. Marini Bettolo Marconi, C. Maggi, M. Paoluzzi, and A. Puglisi, Phys. Rev. Res. **2**, 023321 (2020).
[57] J. Stenhammar, Phys. Rev. Lett. **114**, 018301 (2015).
[58] P. Dolai, A. Simha, and S. Mishra, Soft Matter **14**, 6137 (2018).
[59] A. Das, A. Polley, and M. Rao, Phys. Rev. Lett. **116**, 068306 (2016).
[60] Y. Wang, Z. Shen, Y. Xia, G. Feng, and W. Tian, Chin. Phys. B **29**(5), 053103 (2020).
[61] H. Walter and D. E. Brooks, FEBS Lett. **361**, 135–139 (1995).
[62] A. B. Fulton, Cell **30**, 345–347 (1982).
[63] S. Cayley, B. A. Lewis, H. J. Guttman, and M. T. Record, Jr., J. Mol. Biol. **222**, 281–300 (1991).
[64] S. Boeynaems *et al.*, Trends Cell Biol. **28**(6), 420–435 (2018).
[65] K. E. Handwerger *et al.*, Mol. Biol. Cell **16**, 202–211 (2005).
[66] N. Kedersha *et al.*, J. Cell Biol. **151**, 1257–1268 (2000).
[67] M. A. Andrei *et al.*, RNA **11**, 717–727 (2005).
[68] L. Angelani, C. Maggi, M. L. Bernardini, A. Rizzo, and R. Di Leonardo, Phys. Rev. Lett. **107**, 138302 (2011).
[69] R. C. Krafnick and A. E. Garcia, Phys. Rev. E **91**, 022308 (2015).
[70] J. Chakrabarti, S. Chakrabarti, and H. Lowen, J. Phys.: Condens. Matter **18**, L81–L87 (2006).
[71] J. Dzubiella, J. Chakrabarti, and H. Löwen, J. Chem. Phys. **131**, 044513 (2009).
[72] S. Asakura and F. Oosawa, J. Chem. Phys. **22**, 1255 (1954).
[73] M. D. Gratale, T. Still, C. Matyas, Z. S. Davidson, S. Lobel, P. J. Collings, and A. G. Yodh, Phys. Rev. E **93**, 050601(R) (2016).
[74] G. Meng, N. Arkus, M. P. Brenner, and V. N. Manoharan, Science **327**, 560 (2010).

[75]G. H. Koenderink, G. A. Vliegenthart, S. G. J. M. Kluijtmans, A. van Blaaderen, A. P. Philipse, and H. N. W. Lekkerkerker, Langmuir **15**, 4693 (1999).
[76]A. Stradner, H. Sedgwick, F. Cardinaux, W. C. K. Poon, S. U. Egelhaaf, and P. Schurtenberger, Nature **432**, 492 (2004).
[77]P. Liu, S. Ye, F. Ye, K. Chen, and M. Yang, Phys. Rev. Lett. **124**, 158001 (2020).
[78]F. Smallenburg and H. Lowen, Phys. Rev. E **92**, 032304 (2015).
[79]D. Ray, C. Reichhardt, and C. J. Olson Reichhardt, Phys. Rev. E **90**, 013019 (2014).
[80]R. Ni, M. A. Cohen Stuart, and P. G. Bolhuis, Phys. Rev. Lett. **114**, 018302 (2015).
[81]L. R. Leite, D. Lucena, F. Q. Potiguar, and W. P. Ferreira, Phys. Rev. E **94**, 062602 (2016).
[82]M. Zaeifi Yamchi and A. Naji, J. Chem. Phys. **147**, 194901 (2017).
[83]A. Duzgun and J. V. Selinger, Phys. Rev. E **97**, 032606 (2018).
[84]Y. Hua, K. Li, X. Zhou, L. He, and L. Zhang, Soft Matter **14**, 5205 (2018).
[85]Y. Baek, A. P. Solon, X. Xu, N. Nikola, and Y. Kafri, Phys. Rev. Lett. **120**, 058002 (2018).
[86]N. D. Mermin, Phys. Rev. B **176**, 250 (1968).
[87]W. Lechner and C. Dellago, J. Chem. Phys. **129**, 114707 (2008).
[88]Y. Tang, J. Chem. Phys. **116**, 6694 (2002).
[89]H. Löwen and E. Allahyarov, J. Phys.: Condens. Matter **10**, 4147 (1998).